ICRF HEATING EXPERIMENTS ON JIPP T-II

M. ICHIMURA*, J. FUJITA, S. HIROKURA,
E. KAKO, K. KAWAHATA, Y. KAWASUMI,
A. NISHIZAWA, N. NODA, I. OGAWA, K. OHKUBO,
Y. ONO, M. SASAO, S. SHINOHARA**,
S. TANAHASHI, T. TETSUKA, K. TOI, T. WATARI,
T. AOKI, S. HIDEKUMA

Institute of Plasma Physics,
Nagoya University,
Nagoya, Japan

ABSTRACT. Data of JIPP T-II ICRF heating experiments are presented. The experiment covers three typical cases: the low-concentration hydrogen minority case, the high-concentration hydrogen minority case, and the ^{3}He-minority case. The best heating efficiency is obtained for the ^{3}He-minority case. It is shown through power balance analysis that the two H-minority cases are different in the wave energy deposition profile. The difference is explained by the presence of a local cavity mode in the high-concentration minority case. The ion temperature stops rising at a power density level of 0.65 W·cm^{-3} for the hydrogen minority experiments. No such deterioration is found in the case of the ^{3}He minority experiment up to a power density level of 0.45 kW·cm^{-3}. This is the maximum possible to attain within the maximum power injection (180 kW) up to which the experiment is conducted. An analytic solution of the Fokker-Planck equation is derived in order to interpret the deterioration of the heating efficiency.

1. INTRODUCTION

For the heating of thermonuclear fusion plasma, the use of waves in the ion cyclotron range of frequency (ICRF) offers several advantages. Recent high-power ICRF heating experiments [1–4] have demonstrated the practicability of fast-wave heating with a variety of heating regimes. Based on the success in handling MW level ICRF power injection, the application of ICRF heating to future large tokamaks is becoming realistic. In the Institute of Plasma Physics, Nagoya University, ICRF heating is projected in the R-project proposal. The experiment presented here was carried out on JIPP T-II as a preparatory experiment intended to aid in designing the R-tokamak. One of our interests is the clarification of the wave propagation and absorption mechanisms, which is important in deciding the heating regime best suited to the R-tokamak. Another interest is in the mechanism of deterioration of the heating efficiency which occurs with high-power ICRF heating. It is particularly important to derive a scaling to estimate how much ICRF power will be injected in future devices without deterioration of the heating efficiency. We have reason to believe that the power density will play a key role in limiting the injection power. It is shown in Section 4 through an analysis of experimental data that slipping of minority ions gives rise to a reduced heating efficiency with heating power densities higher than a certain level.

2. EXPERIMENTAL RESULTS

JIPP T-II [5] in the Institute of Plasma Physics, Nagoya University, is a stellarator-tokamak hybrid device with a major radius of R = 91 cm and a minor radius of a = 15 cm. The ICRF heating experiment is carried out in a tokamak operating at a toroidal magnetic field of around 2.7 T and a plasma density ranging from 2 to 5 × 10^{13} cm^{-3}. The plasma current is around 90 kA, and the Joule input power is about 100 kW throughout this experiment. The deuterium

Present and permanent addresses:
* Plasma Research Center, Tsukuba University, Ibaraki 305, Japan.
** Department of Physics, University of Tokyo, Tokyo 113, Japan.

plasma with minority ions of hydrogen or ^{3}He is heated in a two-ion hybrid regime. Frequencies of 40 MHz for the hydrogen minority and 26.7 MHz for the ^{3}He minority are used so that the ion-ion hybrid resonance layer is located near the plasma centre. Two all-metal antennas with Faraday shields are set in the vacuum vessel and each receives RF power from its own oscillator. Each antenna has an all-metal structure with a Faraday shield and consists of a top and a bottom half-turn pair. RF currents are fed from the low-field side near the equatorial plane in order to produce a poloidal m = 0 current loop. The antenna configuration is very similar to that of TFR except that the present antenna covers a greater portion of the low-field side. The experiment is carried out for three cases: 4%H, 10%H, and 10%^{3}He. The concentrations of the minority ions are measured spectroscopically in the H-minority experiments, whereas, in the ^{3}He-minority experiments, they are deduced from an analysis of the gas dynamics.

We regard 4%H and 10%H as typical cases representing low and high concentrations of minority hydrogen ions. A favourable result is obtained in the 4%H experiment: the heating is successful up to a net input power of 260 kW, where the power density is 0.65 W·cm^{-3}; this power corresponds to twice the Joule input power. The deuterium and hydrogen temperatures are measured by a mass-discriminating fast-neutral-particle analyser. As is shown in Fig.1, the deuterium temperature T_D increases from 270 to 570 eV. The heating rate is 1.2 eV·kW^{-1}. The increase in the electron temperature T_e is also found by measuring the electron cyclotron emission calibrated by pulse height analysis of soft X-rays (Fig.2). In this figure, the electron temperature rises with time from 0.78 keV but begins to decrease after reaching a maximum value of 1.1 keV (before the RF pulse is turned off). Application of higher power up to 400 kW (power density of 1 W·cm^{-3}) does not bring about any further increase in T_D, and a deterioration of the confinement is observed. A similar heating rate is also obtained with the 10%H experiment. The deterioration of the heating efficiency occurs, however, at a power level as low as 150 kW. In both cases, the deterioration of heating efficiency is preceded by a deterioration of the electron energy confinement, along with an increased influx of heavy ion impurities.

In the ^{3}He minority case (27 MHz), the maximum injection power is limited to 180 kW because of arcing at high-power injection in the tuner, which has primarily been designed for 40 MHz. However, this power is large enough to allow a reasonable comparison with H-minority experiments as far as heating efficiency is concerned. In the ^{3}He-minority experiment, a heating efficiency (eV·kW^{-1}·cm^{-3}) twice as high as in the H-minority case is observed, demonstrating the superiority of ^{3}He as a minority species for fixed toroidal magnetic field strength. Within this power level, no deterioration of heating efficiency was observed. In Fig.3, the relationship between the power applied and the increase in the deuterium temperature is summarized in terms of $\Delta T_D \bar{n}$.

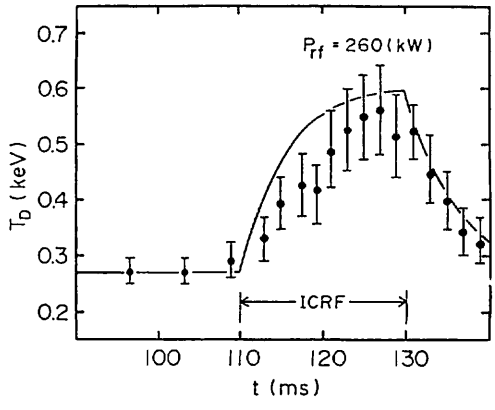

FIG.1. Time evolution of deuterium temperature; solid line is obtained in computing Eq.(1).

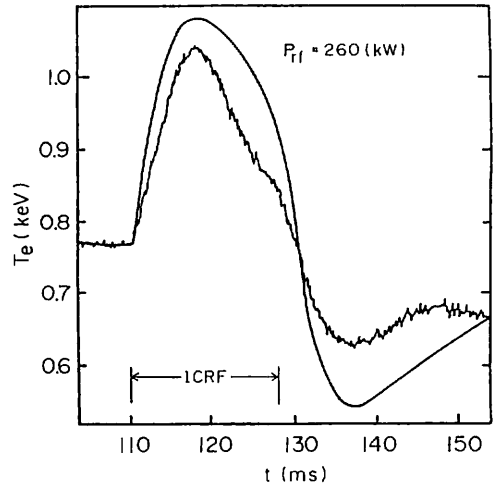

FIG.2. Time evolution of electron temperature; electron temperature rises rapidly with higher RF power and begins to decrease later when RF is still on. Dotted line shows result of simulation calculations with measured radiation loss as input.

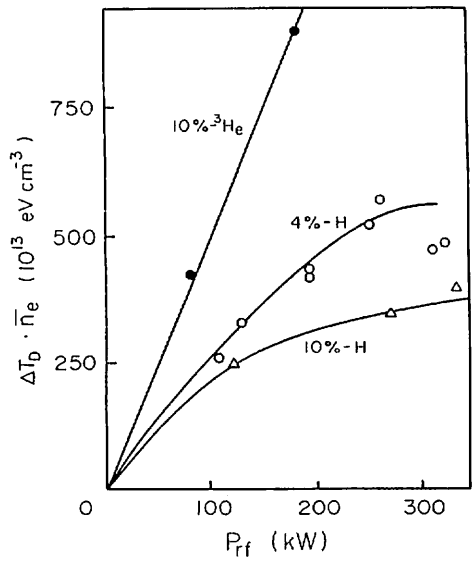

FIG.3. Power dependence of deuterium temperature.

3. ANALYSIS

The reason for the difference between the 4%H and 10%H cases can be understood from an analysis of the usual power balance equations:

$$\frac{d}{dt}(n_H T_H) = -\frac{n_H(T_H - T_D)}{\tau_{HD}} - \frac{n_H(T_H - T_e)}{\tau_{He}} - \frac{n_H T_H}{\tau_H} + \frac{2}{3}\left\langle P_{RF}\right\rangle_H$$

$$\frac{d}{dt}(n_D T_D) = -\frac{n_D(T_D - T_H)}{\tau_{DH}} - \frac{n_D(T_D - T_e)}{\tau_{De}} - \frac{n_D T_D}{\tau_D} + \frac{2}{3}\left\langle P_{RF}\right\rangle_D$$

$$\frac{d}{dt}(n_e T_e) = -\frac{n_e(T_e - T_D)}{\tau_{eD}} - \frac{n_D(T_e - T_H)}{\tau_{eH}} - \frac{n_e T_e}{\tau_e} - \left\langle P_{rad}\right\rangle + \frac{2}{3}\left\langle P_{RF}\right\rangle_e + \frac{2}{3}\left\langle P_J\right\rangle \quad (1)$$

Here, n_H, n_D and n_e are the densities, and T_H, T_D and T_e the temperatures of H, D and e, respectively. τ_H, τ_D and τ_e are the energy confinement times of the respective species. $\langle P_{RF}\rangle_H$, $\langle P_{RF}\rangle_D$ and $\langle P_{RF}\rangle_e$ are the averaged heating power densities on H, D and e, respectively. τ_{HD} and τ_{He} are energy relaxation times from H to D and e, respectively. Similarly, τ_{De} and τ_{DH} are such relaxation times from D to e and H, and τ_{eD} and τ_{eH} are those from e to D and H. $\langle P_{rad}\rangle$ and $\langle P_J\rangle$ are the averaged radiation loss and the Joule input power, respectively. Without RF, the set of Eqs (1) can be solved for τ_H, τ_D and τ_e in the Ohmic-heating phase because $\langle P_{RF}\rangle_H$, $\langle P_{RF}\rangle_D$ and $\langle P_{RF}\rangle_e$ are zero and all the other necessary quantities are easily measured or calculated from them. In the presence of RF, Eq.(1) is solved for $\langle P_{RF}\rangle_H$, $\langle P_{RF}\rangle_D$ and $\langle P_{RF}\rangle_e$, on the assumption that transport coefficients τ_H, τ_D and τ_e do not change on the application of RF. We measure the quantities involved in Eq.(1), waiting for 5 ms after the ICRF heating has been turned on. This time-scale, which is not long compared to the heating time, is chosen so as to be able to neglect possible changes in the transport parameters which might be due to impurity influx or some other unknown reasons. 5 ms is much longer than the time-scales associated with wave propagations (about 2 s) or the

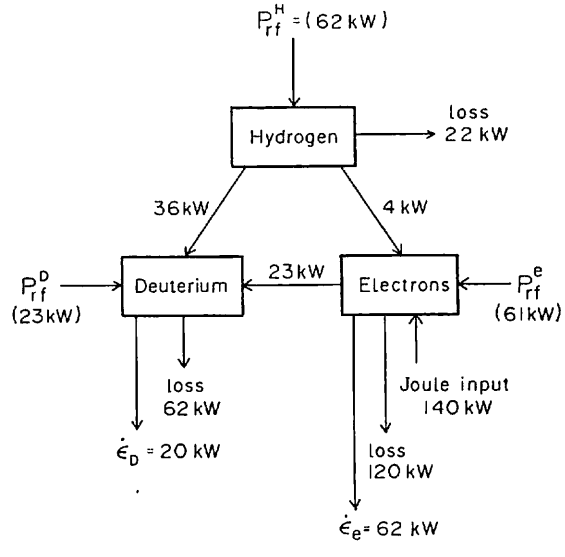

FIG.4. Power balance analysis for 4%H minority case.
$\dot{\epsilon}_D = (3/2)\, n_D T_D V$, $\dot{\epsilon}_e = (3/2)\, n_e T_e V$ (V – plasma volume).

peripheral re-cycling time (about 1 ms); this fact is necessary for minimizing errors arising in estimating the derivative terms in Eq.(1), which might be caused by fluctuations. Throughout this discussion, which is based on a zero-dimensional analysis, a parabolic electron density profile is assumed, and squared parabolic profiles are assumed for T_e, T_H and T_D. An example for the power balance is shown in Fig.4 for the case of the 4%H experiment. The RF powers absorbed by the species as given in the parentheses are calculated on the basis of the known power transfer data. Among the dominant features we find is the fact that not only minority ions but also electrons and deuterons absorb wave energy in the 4%H experiment, while only minority ions absorb a significant amount of wave energy in the 10%H experiments. These results are different from those of TFR and PLT: TFR reports direct heating of electrons in the high-concentration H-experiment, while PLT states that only minority ions are directly heated in the low-concentration H-experiment. Our experimental results are the other way round, in the sense that electron heating is rather observed in low- than in high-concentration H-experiments. The reason for this difference between their and our results can be understood in terms of a wave propagation analysis keeping the differences in the antenna configurations in mind. Our antenna is very similar to the TFR antenna in shape but differs from it in performance. Our antenna is smaller and operates on a lower frequency than that of TFR. So, the RF current on the antenna is shaped to be perfectly uniform in our experiment. The question from which side the wave is incident depends, however, on the local structure of the wave propagation. One of the important parameters characterizing the wave propagation is defined by [4]

$$\epsilon_H^c = \left(\frac{k_\parallel^2 c^2}{\omega_{PD}^2} + \frac{4}{3} \right) \frac{k_\parallel v_T}{\omega} \qquad (2)$$

If the H-concentration ϵ_H, is higher than this critical value ϵ_H^c, there is a mode conversion layer present. Here, ω_{pD} is the deuterium ion plasma frequency, $k_\parallel$ the parallel wave number, v_T the thermal velocity of the hydrogen ions, c the velocity of light, and ω the applied RF frequency. Substituting the values relevant for our experiment on the right-hand side of Eq.(2), we obtain $\epsilon_H^c \approx 2\%$, which is smaller than any H-concentrations we use in this experiment. Therefore, we may assume the presence of a mode conversion layer throughout this experiment. Another important parameter,

$$\eta = \pi \frac{\sqrt{3}}{2\sqrt{2}} R_H \frac{\omega_{pD}}{c} \qquad (3)$$

is known to be a quantity which can be used to measure the separation between a resonance layer and a cut-off layer [6, 8]. Here, R is the major radius. When the value of η becomes larger than unity, a wave incident from the low-field side is completely reflected, and one from the high-field side is almost completely mode-converted. On the other hand, with a value of η less than unity, the mode conversion process is attainable both from the low- and the high-field sides. An examination of Eq.(3) with experimental parameters yields η-values of 0.5 and 1.3 for the 4%H and 10%H cases, respectively. Thus, we interpret the electron part of the wave absorption in the 4%H experiment as a consequence of the mode conversion of a wave to an electrostatic mode. Theoretically, a certain amount of electron heating is expected in the 10%H experiment, as well. This is because the wave energy is incident from the high- as well as from the low-field side: the former has a chance to be mode-converted and to heat the electrons. However, no electron heating is observed experimentally. We assume that the wave radiation primarily consists of waves coming from the low-field side. An indication of this fact is found in the following experimental data: the wave excitation and the propagation characteristics are related to the loading resistance of the antenna. In Fig.5, measured loading resistances are plotted versus

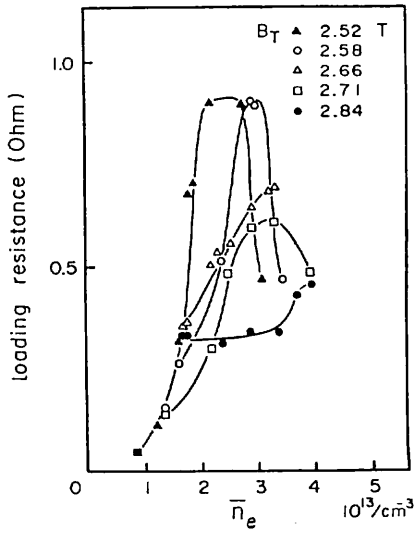

FIG.5. Loading resistance versus $\bar{n}_e$.

the plasma density for the high-concentration minority case. It is an outstanding characteristic of this case that the plasma density which yields the maximum loading resistance increases with increasing toroidal magnetic field strength. This tendency is well understood, provided the local cavity mode predicted by the theory [8–11] is really present; as the toroidal magnetic field B_T increases, the resonance cut-off double layer shifts towards the low-field side, thereby reducing the volume of the cavity. For the RF frequency kept constant, the cavity resonance can only be satisfied by the shorter wavelength realized in the case of higher plasma density. On the basis of this physical picture, we shall draw an analogy with a plasma-filled waveguide of rectangular cross-section. A mean Alfvén wave number $k_{\perp,\omega}$, for fast-wave oscillation is defined by

$$k_{\perp,\omega} = \omega(\mu_0 \bar{n} m_D/\bar{B}^2)^{1/2} \qquad (4)$$

where the averaged number density, $\bar{n}$, and the averaged magnetic field, $\bar{B}$, are calculated from the experimental data at the cavity resonance. Here, m_D is the deuteron mass. A geometric wave number $k_{\perp,g}$, which characterizes the cross-section of the cavity and the fundamental resonance condition, is defined by

$$k_{\perp,g} = \frac{\pi}{2}(a^{-2} + b^{-2})^{1/2} \qquad (5)$$

where a and b are the dimensions of the cavity as estimated from the computed cut-off surfaces. This simple model would predict a linear relationship between $k_{\perp,\omega}$ and $k_{\perp,g}$ at the fundamental resonance. The relationship between $k_{\perp,\omega}$ and $k_{\perp,g}$ obtained experimentally is plotted in Fig.6, where the straight line represents a best-fit relationship of $k_{\perp,\omega}/k_{\perp,g} = 0.6$. These results confirm the presence of a cavity mode on the low-field side, in the case of high-H minority concentration. The increase in the loading resistance of the low-field side part of an antenna when a local cavity mode is present is consistent with the results obtained by running Lapièrre's code [9]. Thus, it is possible that the major part of the wave energy is emitted from the low-field side. The wave energy is then absorbed in the cyclotron layer by minority ions. Thus the reason for the difference between the JIPP T-II and TFR results is comprehensible. This contrasts with the case where the concentration of the minority ions is low; there is only a weak connection between $k_{\perp,\omega}$ and $k_{\perp,g}$. In this case, the wave is not localized, and it is then absorbed in the mode conversion layer.

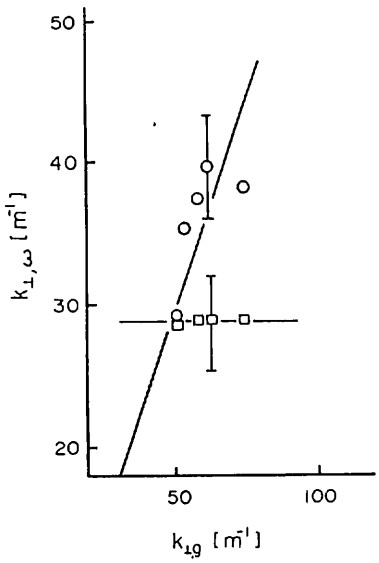

FIG.6. Relation between Alfvén wave number $k_{\perp,\omega}$ and geometric wave number $k_{\perp,g}$.

4. DISCUSSION

The sum of the RF powers absorbed by the respective species is less than that radiated from the antennas. If efficiency is defined by

$$\gamma = \left(\langle P_{RF}\rangle_e + \langle P_{RF}\rangle_H + \langle P_{RF}\rangle_D\right) \Big/ \langle P_{RF}\rangle \qquad (6)$$

We obtain $\gamma = 0.56$ for the 4%H and $\gamma = 0.23$ for the 10%H case. In the following discussions, the Fokker-Planck equation is used to interpret an efficiency smaller than unity. It is well known that the particle confinement is determined by the plasma current, which is only 90 kA in this experiment: particles with an energy of more than 20 keV cannot be confined. It is, therefore, important to gain some insight into the behaviour of the minority ions which are intensively heated and finally lost. An analytic steady-state solution of the linear Fokker-Planck equation was first given by Stix [12]. It is, however, not complete because the particle flow through velocity space is neglected. According to the Stix notation, the isotropic linear Fokker-Planck equation with a quasi-linear collision term is written in the form:

$$\frac{\partial A}{\partial t} = \frac{1}{v^2}\frac{\partial}{\partial v}[-v^2\Gamma] \qquad (7)$$

where

$$\Gamma = -\frac{1}{v^2}\left[-\alpha v^2 + \frac{1}{2}\frac{\partial}{\partial v}(\beta v^2)\, A + \left(\frac{1}{2}\beta + K\right) v^2 \frac{\partial A}{\partial v}\right] \tag{8}$$

The first integral of Eq.(7) gives

$$-v^2\Gamma = c_1 \tag{9}$$

Here, c_1 has a physical meaning of particle flow through the velocity space, which has been ignored in Ref.[10]. If it is retained, the solution of Eq.(7) has the form

$$A(v) = c_1 \int_v^{v_0} \frac{1}{\left(\frac{1}{2}\beta + K\right)V^2} \frac{1}{A_0(V)}\, dV\, A_0(V) \tag{10}$$

where

$$A_0(V) = \exp\left(-\int_0^v \frac{-V^2}{\frac{1}{2}\beta + K}\, dV\right) \tag{11}$$

is the solution from Ref.[10], and

$$v_0 = (2E_{max}/m)^{1/2} \tag{12}$$

with E_{max} the maximum energy of particles which can be confined in the system. A numerical comparison of analytical expressions (10) and (11) with experimental parameters yields A(v) quite different from $A_0(v)$, implying the importance of the particle flow through the velocity space. The distribution function of the minority ions A(v) is far from a Maxwellian distribution. We deduce an effective ion temperature from the inclination of the theoretically obtained distribution function around the energy range where the fast-neutral-particle analyser works in the experiment. The power dependence of the hydrogen temperature is compared to the dependence as predicted by theory in Fig.7; we see that there is a qualitative agreement. The particle energies transferred from hydrogen to deuterium by the relaxation process, P_{DH}, and from hydrogen to the electrons, P_{eH}, are given by

$$P_{DH} = \int_0^{v_0} 4\pi \frac{m}{2} v^2 \frac{\partial}{\partial v}\left[-\alpha_D v^2 + \frac{1}{2}\frac{\partial}{\partial v}(\beta_D v^2)\, A + \frac{1}{2}\beta_D v^2 \frac{\partial A}{\partial v}\right] \tag{13}$$

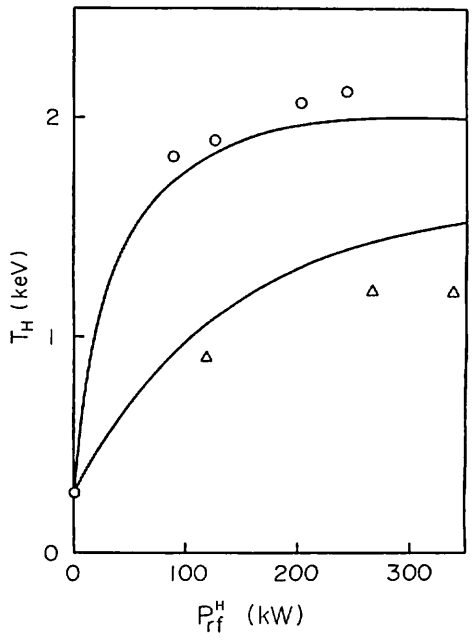

FIG. 7. Temperature of minority ions versus input RF power. Open circles and triangles show measured minority ion temperature for 4%H and 10%H cases, respectively. Solid lines designate theoretical calculations from Eq.(10).

$$P_{eH} = \int_0^{v_0} 4\pi \frac{m}{2} v^2 \frac{\partial}{\partial v}\left[-\alpha_e v^2 A + \frac{1}{2}\frac{\partial}{\partial v}(\beta_e v^2) A + \frac{1}{2}\beta_e v^2 \frac{\partial A}{\partial v}\right] dv \tag{14}$$

$$\langle P_{RF}\rangle = \frac{3}{2} mnK \tag{15}$$

and we notice an obvious relation

$$\langle P_{RF}\rangle = \langle P_{DH}\rangle + \langle P_{eH}\rangle + c_1 E_{max} \tag{16}$$

where the last term is the portion of the energy lost as energetic ions. The portion of the wave energy absorbed by hydrogen and then transferred to deuterium ions and electrons is given by

$$\xi = \frac{\langle P_{DH} + P_{eH}\rangle}{\langle P_{RF}\rangle_H} = \frac{\langle P_{RF}\rangle - c_1 E_{max}}{\langle P_{RF}\rangle_H} \tag{17}$$

Since the loss term $c_1 E_{max}/\langle P_{RF}\rangle_H$ is an increasing function of $\langle P_{RF}\rangle_H$, ξ becomes small on high-power heating. The result of the numerical computation of ξ

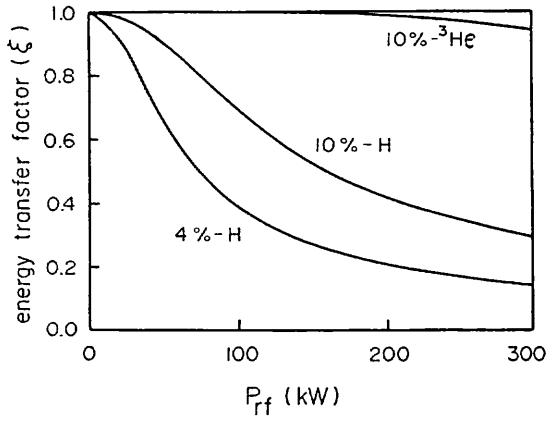

FIG.8. Energy transfer factors of minority ions.

is shown in Fig.8 for three cases: 4%H, 10%H and 10%^{3}He. It is worthwhile mentioning that, for the 10%H case, the application of a power over 150 kW does not serve to heat D but only to increase the particle loss of minority hydrogen. This may be the reason why we observe a deterioration of the heating efficiency in the experiment at a higher power level. We also find that the threshold is as low as 30 kW in the case of the 4%H experiment. However, the ion temperature continues to rise together with increasing power from this power level up to 260 kW because the wave deposits its energy not only on H but also on e and D. The 10%^{3}He experiment belongs to the high-concentration minority case and compares well with the 10%H experiment. In this case, the threshold is high enough for no deterioration to occur, and the high heating efficiency is maintained. This superiority of ^{3}He as a minority species is attributed to the larger collisional cross-section of ^{3}He than that of H.

We observe in this experiment that the deteriorating effect of RF first affects the electron energy confinement. This is due to the enhanced radiation loss. The origin of the impurity is sought by examining the visible light emission which is indicative of the impurity influx and the characteristic lines in soft-X-ray emission which yield information on the core impurity. The radiation loss is mainly due to impurities of the heavy metals Ti and Mo, the former coming from the vacuum wall and the latter from the limiter. The bolometrically measured radiation loss increases gradually with time for about 10 ms; this is in contrast with the rise-time for visible light, which is 1 ms. A simulation using Eq.(1) with the measured radiation loss gives the solid curves shown in Figs 1 and 2. Thus, the behaviour of the electron temperature is well understood in terms of the radiation loss. Though the deterioration of electron energy confinement does not affect the ion heating significantly, impurities are another problem to be solved in experiments in the near future.

5. SUMMARY

The experimental results of ICRF heating on JIPP T-II were described and three typical heating regimes were compared. The highest heating efficiency was achieved in the ^{3}He-minority experiment. In the H-minority experiment, low- (4%H) and high-concentration minority (10%H) cases were compared. Differences were found in the wave energy deposition profile on each species derived through power balance analysis. This difference was explained in terms of mode coversion theory; this model was consistent with the measured loading resistance. The behaviour of the plasma under high-power ICRF heating was also investigated with power levels of up to 400 kW. A deterioration in the heating efficiency was observed in both cases with a heating power density less than 0.65 W·cm^{-3}. The mechanism of the heating deterioration was explained in terms of a relaxation process with a solution of the Fokker-Planck equation.

ACKNOWLEDGEMENTS

The authors are indebted to Drs T. Sato and K. Adati for providing us with the RFC-XX RF power sources. They are grateful to Drs T. Hamada, K. Matsuura, R. Sugihara, and T. Amano for continuous encouragement and useful discussions. They also would like to thank M. Mugishima and H. Ishiguro for the operation of the FW generator.

REFERENCES

[1] HWANG, D., BITTER, M., BUDNY, R., CAVALLO, A., CHRIEN, R., et al., in Plasma Physics and Controlled Nuclear Fusion Research (Proc. 9th Int. Conf. Baltimore, 1982), Vol.2, IAEA, Vienna (1983) 3.
[2] EQUIPE TFR, ibid., 17.
[3] KIMURA, H., MATSUMOTO, H., ODAJIMA, K., KONOSHIMA, S., YAMAMOTO, T., et al., ibid., 113.
[4] JACQUINOT, J., McVEY, B.D., SCHARER, J.E., Phys. Rev. Lett. 39 (1977) 88.

[5] FUJITA, J., ITOH, S., KADOTA, K., KAWAHATA, K., KAWASUMI, Y., et al., in Plasma Physics and Controlled Nuclear Fusion Research (Proc. 8th Int. Conf. Brussels, 1980), Vol.1, IAEA, Vienna (1981) 209.
[6] SWANSON, D.G., Phys. Rev. Lett. **36** (1976) 316.
[7] SCHARER, J.E., McVEY, B.D., MAU, T.K., Nucl. Fusion **17** (1977) 297.
[8] COTSAFTIS, M., SY, W.N-C., Phys. Lett. **93A** (1983) 193.
[9] LAPIERRE, T., in Heating in Toroidal Plasmas (Proc. 2nd Joint Grenoble-Varenna Int. Symp., Como), Vol.1 (1980) 549.
[10] FUKUYAMA, A., NISHIYAMA, S., ITOH, K., ITOH, S-I., Nucl. Fusion **23** (1983) 1005.
[11] ITOH, K., ITOH, S-I., FUKUYAMA, A., Nucl. Fusion **24** (1984) 13.
[12] STIX, T., Nucl. Fusion **15** (1975) 737.

(Manuscript received 11 October 1983
Final manuscript received 2 May 1984)